

INSAR HEIGHT INVERSION BY USING 3-D PHASE PROJECTION WITH MULTIPLE BASELINES

B.-I. Wu, M. Yeung, Y. Hara [†], and J. A. Kong

Massachusetts Institute of Technology
USA

Abstract—This study introduces the notion of 2-D and 3-D Phase Projection in our search for a simple and elegant solution to further reduce noise during InSAR post-processing steps with multiple baselines. Projection is a powerful tool to reduce noise in a system of more than two satellites. It does so by noting that the geometry of the satellite configuration restricts the range of values over which the wrapped phases can assume. Projection in general reduces noise in the system by utilizing the information provided by the configuration of the satellites to reduce the set of allowed phase points, thereby improving the robustness of the system in the presence of noise. Our results show that, for most cases, whether with the extremely small baseline distance or non-integer baseline ratios, using 3-D Projection gives better height inversion results.

1. INTRODUCTION

A big problem in interferometry has been to figure out how to reduce noise in a system of satellites [1–4]. Correct height retrieval is an integral part of many applications using InSAR, such as remote sensing [5, 6], and data correction using multiple satellites may also benefit other SAR applications [7–9]. Simple ways like using a low-pass (averaging) filter have been proposed, and they work well sometimes. However, one can do better if there are more than 2 satellites in place. Let us assume that we have 3 satellites, although the argument would hold with more satellites as well. The presence of 3 satellites gives us a whole new dimension to work with: When there are only 2 satellites, there just isn't an extra degree of freedom that can help us narrow down

Corresponding author: B.-I. Wu (biwu@mit.edu).

[†] Also with Mitsubishi Electric Corporation.

the effects of noise. However, when we introduce an extra satellite, the very position of this third satellite should give us information on whether the unwrapped phase data is coherent. This promises to be a powerful tool to mitigate noise in our system: Since noise is assumed to be randomly distributed but data are not, the partial effects of noise might be picked up and corrected more easily if we use 3 satellites instead of 2. A big portion of this paper will be devoted to investigating this work.

2. 2-D PROJECTION METHOD

In this section, we investigate a noise-reduction technique when 3 satellites are present in a system. This technique, called Phase Projection or simply Projection, is a powerful tool that can potentially lead to increased robustness of the InSAR height retrieval process [10–12]. In essence, projection relies on the very configuration of the satellites to deduce the behavior of the phases, and thus, gives us the ability to classify any other behavior of the phases as the actions of noise. Because projection relies heavily on the physical configuration of satellites, the method inevitably will be jeopardized when the configuration itself is noisy or not ideal. Nonetheless, we press ahead to investigate how projection can help reduce noise in a multibaseline system. Figure 1 shows the 3 satellite configuration.

The values of the parameters used are shown below.

Table 1. Values of baseline lengths used for 3 baselines.

Parameter	Value Used
B_{12} (m)	150
B_{23} (m)	50
B_{13} (m)	200
α (degrees)	35
Δx (m)	5
X (m)	$3 \cdot 10^5$
H (m)	$5 \cdot 10^5$
Δy (m)	5
Y (m)	$3 \cdot 10^5$
λ (m)	0.03 (<i>X</i> -band)

Note that $B_{13} = B_{23} + B_{12}$, as required by the geometry. To

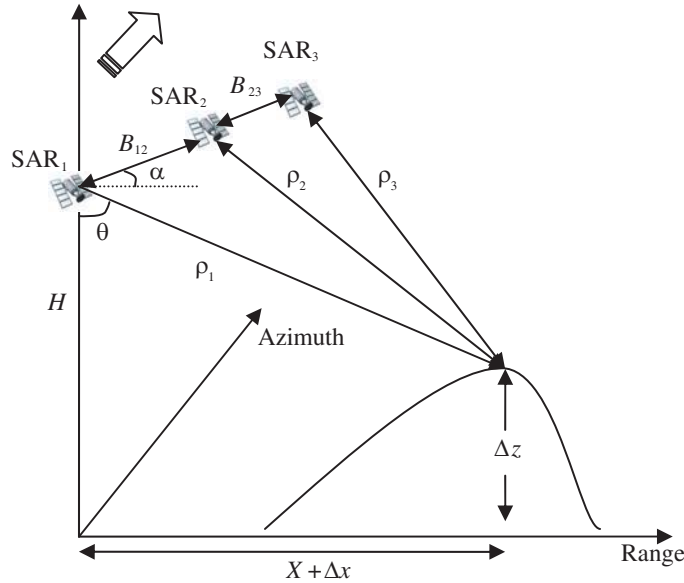


Figure 1. InSAR configuration for 3 satellites, collinear arrangement.

study the configuration in details, consider the following close-up of the 3 antennas:

Since the slant ranges (ρ_1 , ρ_2 , and ρ_3) are on the order of 10^5 m while the baselines (B_{12} , B_{23} , and B_{13}) are on the order of 10^2 m, the slant range vectors to be essentially parallel to one another. This in essence means there are 3 similar triangles that make up the geometry of the satellites, each identified by a baseline. The actual phase values and slant range differences are related by the following simple equation:

$$\phi_{12,13,23} = \frac{4\pi}{\lambda} \Delta\rho_{12,13,23} \quad (1)$$

Since phase values are always measured as wrapped values, Equation (1) decomposes into the following:

$$\psi_{12,13,23} + k_{1,2,3} \cdot 2\pi = \frac{4\pi}{\lambda} \Delta\rho_{12,13,23} \quad (2)$$

In addition, by the rule of similar triangles, the slant range differences and baselines have to be related by simple ratios:

$$\frac{B_{12}}{\Delta\rho_{12}} = \frac{B_{13}}{\Delta\rho_{13}} = \frac{B_{23}}{\Delta\rho_{23}} \quad (3)$$

Thus, we have the following relationships between the wrapped phase values, which we measure, and the baseline lengths, which we know:

$$\frac{\psi_{13} + k_2 \cdot 2\pi}{\psi_{23} + k_3 \cdot 2\pi} = \frac{B_{13}}{B_{23}} \equiv \text{URM}_1 \quad (4a)$$

$$\frac{\psi_{12} + k_1 \cdot 2\pi}{\psi_{23} + k_3 \cdot 2\pi} = \frac{B_{12}}{B_{23}} \equiv \text{URM}_2 \quad (4b)$$

From Equation (4a), it is clear that the wrapped phase ψ_{13} is a linear function of ψ_{23} , with the slope being URM_1 , where URM stands for Unambiguous Range Magnification [13]. Since both ψ_{13} and ψ_{23} are wrapped values, they are bound within a 2-D space of length 2π . Xu et al. were the first to process these wrapped phases in this manner to achieve an URM bigger than 2π [13], and it is known that as long as URM is a rational number, the number of line segments will be finite, i.e., they will reconnect in a wrapped sense when they hit the edges of the domain. Theoretically, the URM technique allows us to expand the unambiguous range to any arbitrary size — just by increasing the ratio of B_{13} to B_{23} . However, when there is noise in the system, points will get shifted away from the line segments (Figure 3). Points that do not lie on a line segment will be inconsistent with Equations (4a) and (4b), which are derived purely from the geometry of the satellite

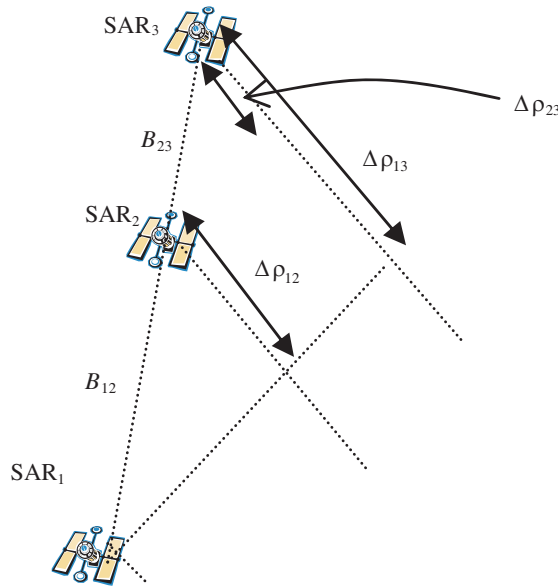


Figure 2. Close-up of the 3 InSAR antennas of Figure 1.

configuration. This is thus a clear indication that noise has disrupted the real values of the wrapped phases. Xu et al. [14] suggested that the best way to resolve this problem is to use the “Projection Method” — whenever a point lies away from a line segment, we place it back onto the nearest line segment with the shortest Euclidean distance. This ensures that the phase values maintain consistency of the geometry of the 3-satellite configuration, and also allows us to place the phase points closer (or even onto) the actual wrapped points. Figure 3 shows this process in action.

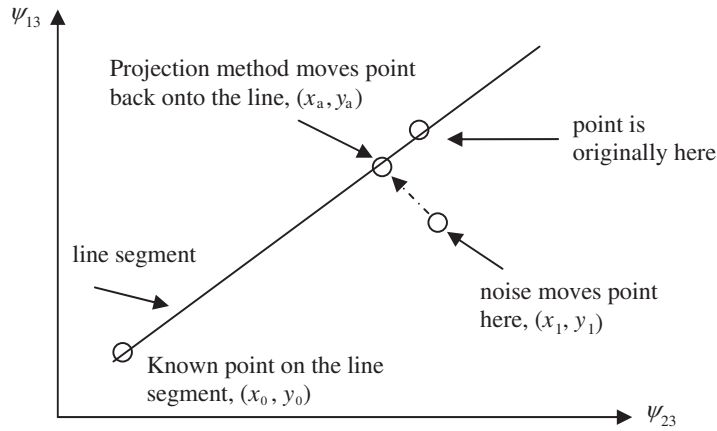


Figure 3. Illustration of the projection method.

Now, we try to frame the 2-D Projection in a solid, mathematical framework. Referring to Figure 3, we name a few key points on the diagram by the following names:

1. A known point on the line segment is defined as (x_0, y_0)
2. An actual ψ_{23} - ψ_{13} phase couplet defined by the interferogram is defined as (x_1, y_1)
3. The point that we want to find, i.e., the point on the line segment that is of the shortest Euclidean distance to (x_1, y_1) is defined as (x_a, y_a) .

With that, we get the following closed form expressions:

$$x_a = \frac{x_1 - \text{URM}_1 \cdot y_0 + \text{URM}_1 \cdot y_1 + \text{URM}_1^2 \cdot x_0}{1 + \text{URM}_1^2} \quad (5)$$

$$y_a = \text{URM}_1 \cdot (x_a - x_0) + y_0 \quad (6)$$

One important thing to note is that since there are going to be more than 1 line segment in the plane, there will also be more than one

possible (x_a, y_a) points that (x_1, y_1) can map to. Since we are only interested in mapping to the line segment that is nearest to (x_1, y_1) , we only need to calculate the distances between (x_1, y_1) and all possible (x_a, y_a) pairs:

$$distance = \sqrt{(x_a - x_1)^2 + (y_a - y_1)^2} \quad (7)$$

and pick the appropriate pair. As an example, Figure 4 illustrates phases with noise of 30 degrees, while Figure 5 shows the results after implementing projection.

We can qualitatively see the inverse relationship between phase noise and effectiveness of Unambiguous Range Magnification. With a larger and larger URM value, the ψ_{13} - ψ_{23} plane gets more and more cluttered with line segments, which would mean a larger and larger unambiguous interval for the phases. In the noiseless case, this would be ideal. However, in the presence of noise, points are shifted away from the line segments. If URM is large, the high density of line segments implies that the distance between 2 adjacent line segments is small. If the noise is high or the URM is high, we could very well be moving points onto the wrong line segments since the segments are so close to one another. The assumption that the closest line segment is where the noisy point originally came from will therefore be wrong,

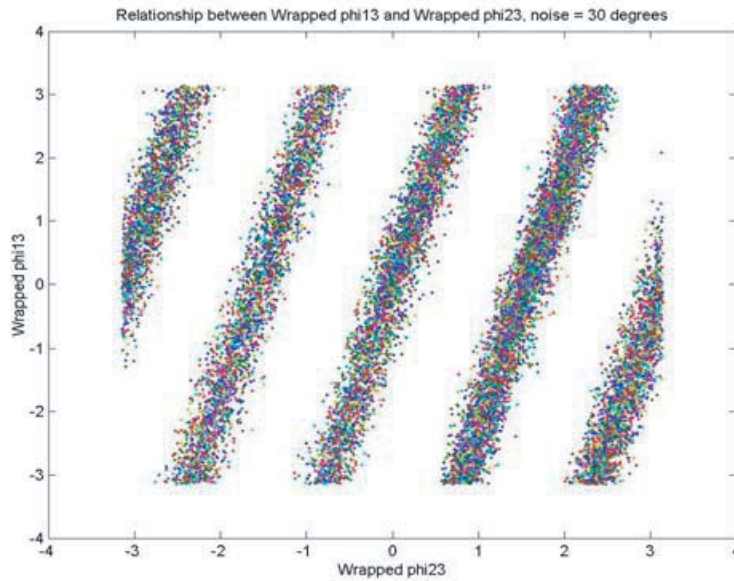


Figure 4. ψ_{13} and ψ_{23} after noise of 30 degrees is added.

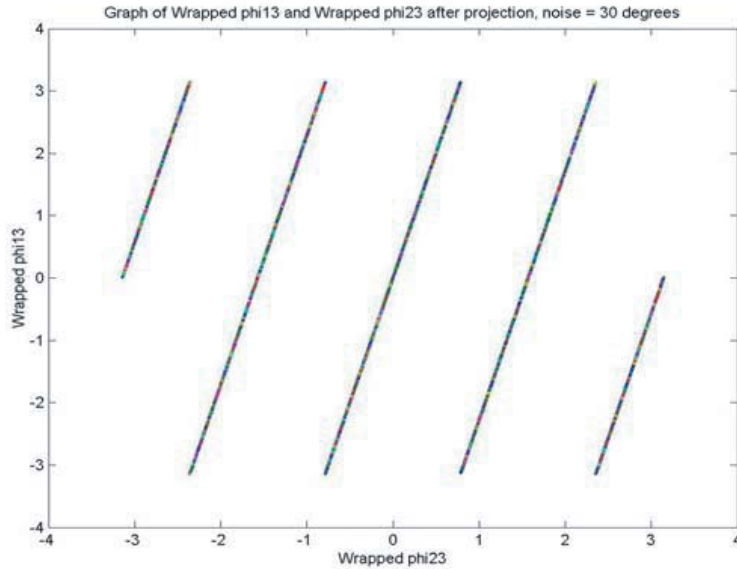


Figure 5. Figure 4 after points are projected onto line segments.

and we would have introduced even more noise into the system than if we had just left the points where they were. Therefore, we cannot make the URM arbitrarily large without eroding the noise budget — a clear engineering trade-off. Up to this point, we have assumed that our baseline ratios (which are equivalent to the URM ratios by Equations (4a) and (4b)) are integers. However, as mentioned before and also in [13], there will be a finite number of line segments as long as the URM ratio is in the set of rational numbers (of which the set of integers is a subset). We now investigate the scenarios under which URM is a non-integer rational number. Since every rational number can be expressed as a ratio of 2 integers, we let $\text{URM} = \frac{p}{q}$, where p and q are both elements of the set of non-zero integers. Then, Equation (4a) becomes:

$$\frac{\psi_{13} + k_2 \cdot 2\pi}{\psi_{23} + k_3 \cdot 2\pi} = \frac{p}{q} \quad (8)$$

The k 's merely denote that the phases are wrapped. After we link the line segments together and plot ψ_{13} against ψ_{23} , the resulting line will have a slope of $\frac{p}{q}$. This means that after linking, the unambiguous range for the horizontal axis is expanded $q \cdot 2\pi$ times, while that for the vertical axis is expanded $p \cdot 2\pi$ times. This has some obvious consequences:

1. If we want to expand the range of ψ_{13} by 4 times, we can use a baseline ratio of $\frac{4}{3}$ instead of $\frac{4}{1}$, which allows us to place the satellites much closer to each other and hence ensuring good coherence between the signals.
2. The drawback of using non-integer values of URM to achieve point 1 is that you now have a higher density of lines wrapped in the 2π by 2π box in the first place. From the previous section, we discussed that a higher density of lines leads to a degradation of noise budget.

In addition, if $\frac{p}{q}$ is a rational number close to an integer (e.g., 2.8), several line segments would appear very close to one another. Figure 6 shows the line segments for $B_{13} = 125$ m, $B_{23} = 50$ m, which means a $\frac{p}{q}$ of $\frac{5}{2}$. Note the increased density of lines, as well as the increased unambiguous range for both the phase values of the horizontal and vertical axes. Figure 7 shows a $\frac{p}{q}$ of 2.8.

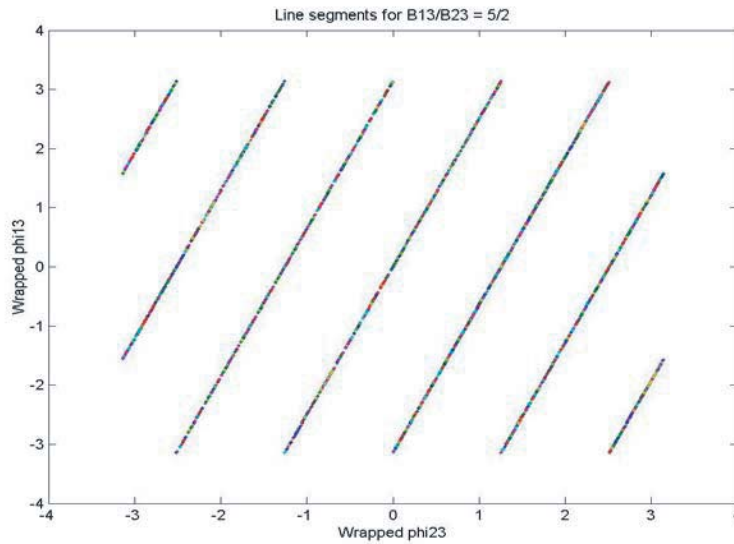


Figure 6. Line segments in the ψ_{13} - ψ_{23} plane with a URM = 2.5.

We can introduce the notion of “noise distance” to describe the phenomenon of decreasing noise budget in exchange for a larger unambiguous range. The noise distance, d_n , is defined as 1/2 of the shortest straight line distance (in radians) between 2 adjacent line segments in the 2π by 2π box, as shown in Figure 8. Qualitatively, this tells you how much the points can deviate from the line segments before they become too close to the adjacent line segment, and thus

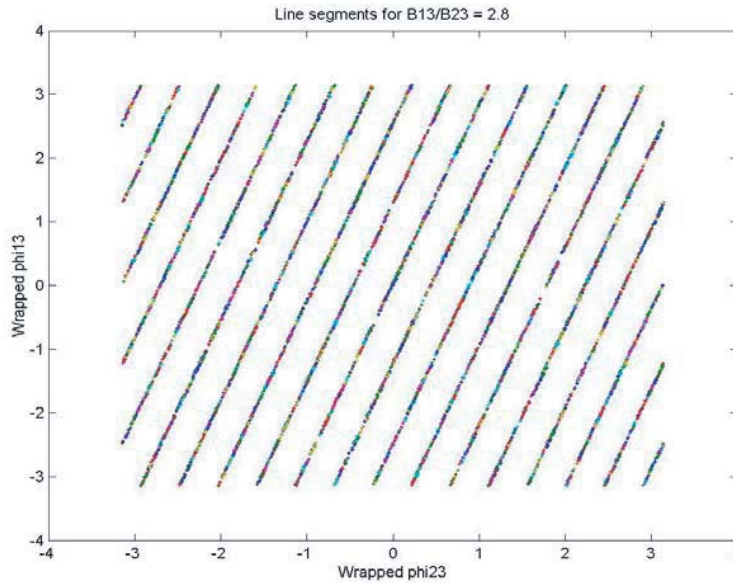


Figure 7. Line segments in the ψ_{13} - ψ_{23} plane with a URM = 2.8.

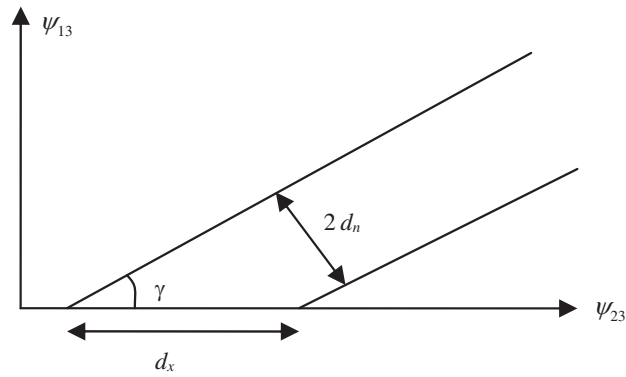


Figure 8. Illustration of the “noise distance” d_n .

when adjusted, will get mapped onto a wrong line segment and thus a wrong ψ_{13} - ψ_{23} value pair.

The noise distance d_n can be shown as the following:

$$d_n = \frac{1}{q} \frac{\pi}{\text{URM}} \sin(\tan^{-1}(\text{URM})) \tag{9}$$

The implication of Equation (9) is clear. A small d_n (something we do

not want) will appear if q is large, and that easily happens if our URM ratio is some rational number which has a large integer denominator when it is expressed as a ratio of integers. Noise budget is really high for integer values and rational numbers that can be expressed as ratios of very small integers (e.g., 1, 2, 3, 1.5, 2.5, 1.2, etc.), but it degrades significantly when the URM ratios become ratios of huge integer numbers.

3. 3-D PROJECTION METHOD

Xu et al. only suggested using a 2-D (i.e., ψ_{13} and ψ_{23} , ψ_{12} and ψ_{23}) plane to place points back onto the line segments. However, it is intuitive to see that we should not be projecting points in the ψ_{13} - ψ_{23} plane independently from those in the ψ_{12} - ψ_{23} ; after all, they share the ψ_{23} axis; and you can easily get any phase difference value, e.g., ψ_{23} if you know the other 2 phase difference values, ψ_{13} and ψ_{12} . Projecting the points in the 2 planes independently will hence cause inconsistent phases that do not obey the geometry of the satellite equation. Although we are not using any value of ψ_{23} to construct our final heights, it seems that resolving this inconsistency may help to achieve more accurate results, since that further adheres to the geometry of the satellite configuration. As such, we propose to apply the projection method in the 3-D space of ψ_{13} - ψ_{12} - ψ_{23} .

We can make the following statements regarding 2-D and 3-D Projection:

1. 2-D Projection moves the noisy points back onto the nearest line segment in the 2-D plane.
2. When viewed from another angle, the noisy point is really not on the line segment at all; it only looks as if it is on the segment if viewed down the correct plane.
3. 3-D Projection truly moves the noisy point onto the line segment (the point is on the line no matter from which angle you are looking at).

The line segments guarantee consistency as is defined by the satellite configuration (Equation (2)), and so only 3-D Projection satisfies the consistency requirement.

The line segments are shown in Figure 9, while Figure 10 shows the noisy points scattered around the line segments. Figure 11 shows the noisy points after 3-D Projection is performed.

Once again, just like 2-D Projection, we would want to frame 3-D

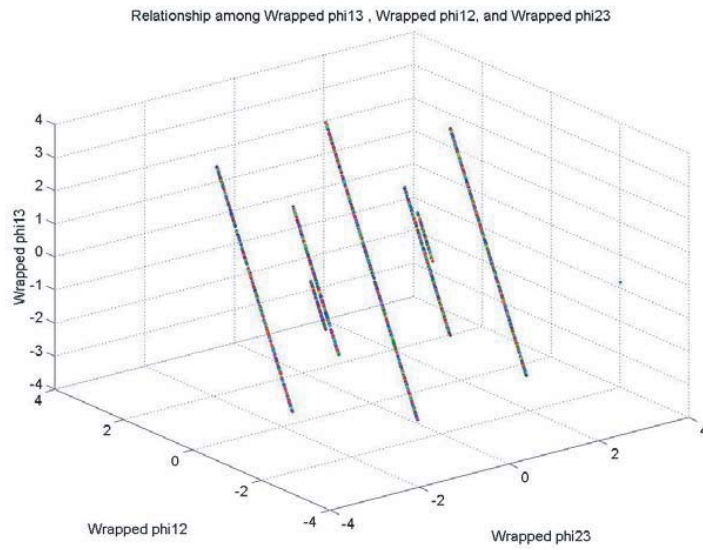


Figure 9. Line segments in the ψ_{13} - ψ_{12} - ψ_{23} space.

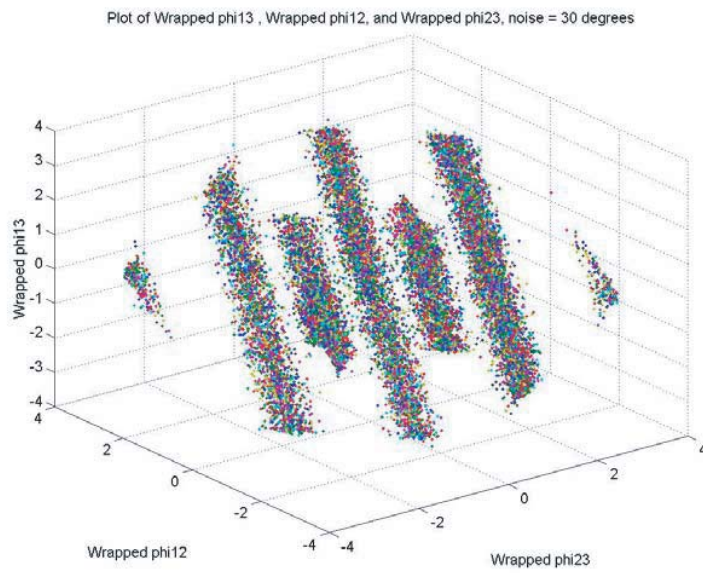


Figure 10. Noisy points in the ψ_{13} - ψ_{12} - ψ_{23} space (noise = 30 degrees).



Figure 11. Figure 10 after points are projected back onto line segments.

projection in a solid, mathematical framework.

$$x_a = \frac{x_1 - \text{URM}_1 \cdot y_0 + \text{URM}_1 \cdot y_1 + \text{URM}_1^2 \cdot x_0 + \text{URM}_2^2 \cdot x_0 - \text{URM}_2 \cdot z_0 + \text{URM}_2 \cdot z_1}{1 + \text{URM}_1^2 + \text{URM}_2^2} \quad (10)$$

$$y_a = \text{URM}_1 \cdot (x_a - x_0) + y_0 \quad (11)$$

$$z_a = \text{URM}_2 \cdot (x_a - x_0) + z_0 \quad (12)$$

One important thing to note is that since there are going to be more than 1 line segments in the plane, there will also be more than one possible (x_a, y_a, z_a) points that (x_1, y_1, z_1) can map to. Since we are only interested in mapping to the line segment that is nearest to (x_1, y_1, z_1) , we only need to calculate the distances between (x_1, y_1, z_1) and all possible (x_a, y_a, z_a) triplets:

$$\text{distance} = \sqrt{(x_a - x_1)^2 + (y_a - y_1)^2 + (z_a - z_1)^2} \quad (13)$$

and then pick the appropriate triplet. All this is analogous to our mathematical formulation of 2-D Projection. There is one subtle, though nevertheless critical, point that we have not taken into

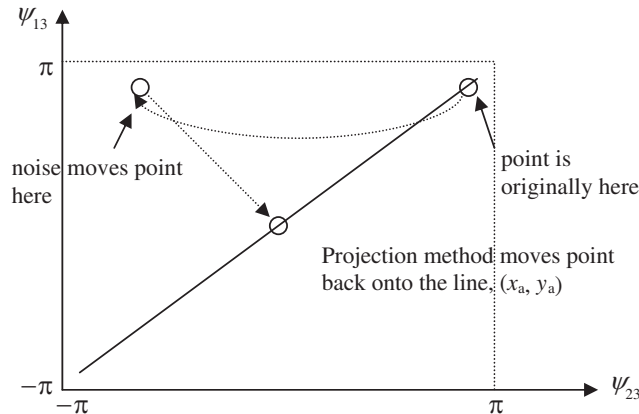


Figure 12. Illustration of a possible scenario during projection.

consideration. Observe the following figure, which illustrates a possible scenario when noise is added to a system.

In Figure 12, imagine a point originally on the line segment as shown. A tiny bit of noise added to the system disrupts the point, such that the point is moved outside of the 2π by 2π box. Because of the wrapping process, the point is now mapped onto some place far away from where it should be. In essence, a tiny bit of noise has been magnified by the projection process.

This problem can actually be solved relatively easily, as long as we know that it does exist. In the scenario offered in Figure 12, suppose that we now introduce one more line segment **outside** of the 2π by 2π box. This new line segment is exactly like that shown in Figure 12, except that it is shifted to the left by 2π . Figure 13 illustrates this issue.

As shown in the figure above, the replication of the original 2π by 2π box in the region outside leads to a projection that, when wrapped back, produces results much closer to the original value. This is critical, as it further improves the value of projection in both 2-D and 3-D algorithms. We also have to recognize that the original 2π by 2π box has to be replicated in all directions so as to perform the best possible job in noise rejection. To accomplish such an end means that in 2-D Projection, we would need an extra 8 2π by 2π boxes in addition to the original one. In 3-D Projection, we would need an extra 26 2π by 2π by 2π cubes in addition to the original one. These additional boxes or cubes would have the same line segments (i.e., same slopes and same relative positions) as those in the original one, just shifted by the appropriate distances.

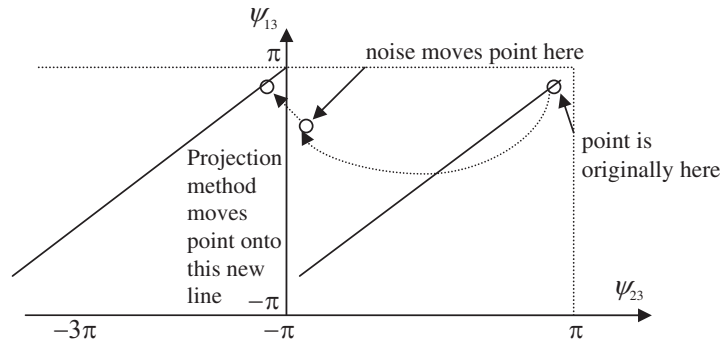


Figure 13. Illustration of Figure 12, with an extra line segment placed outside of original 2π by 2π box.

4. 3-D PHASE PROJECTION FOR A CARTWHEEL CONFIGURATION OF SATELLITES

Now, we step beyond what the previous section has considered and investigate the case where the satellites are fixed in a cartwheel [15], and rotate about a fixed point as they fly in the azimuthal direction. We utilize the cartwheel for the purpose of obtaining all the possible URM ratios. By rotating them as they fly, every single URM ratio can be obtained by virtue of the changing baseline ratios due to the rotation of the cartwheel. Figure 14 below shows this setup.

One thing to take note of is that we have really assumed that the cartwheel is much, much smaller in size than any other distances that

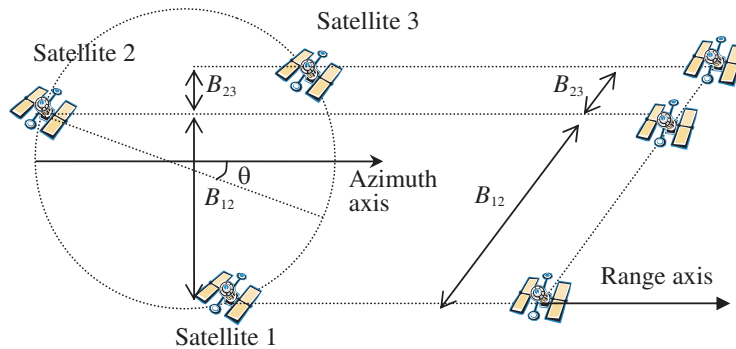


Figure 14. Illustration of cartwheel configuration that allows full range of URM values.

we care about, e.g., the range distance and the height of the satellites above ground. In such a scenario, the 3 satellites are essentially at the same point in space in the azimuth-height plane, and so the cartwheel configuration collapses to a two dimensional problem as desired. This approximation is good so long as that assumption holds true. However, if satellites start to get further and further away, serious problems may arise in our assumptions. For the remainder of the paper, we will take it that those approximations hold.

First, we need a mathematical relationship that describes the transformation from the tilt angle θ to the URM ratios. Letting the shortest straight-line distance between any pair of satellites be R , it is fairly straightforward to show that the relationship is as follows:

$$B_{13} = R \cos(\theta) \quad (14)$$

$$B_{12} = R \cos\left(\frac{\pi}{3} - \theta\right) \quad (15)$$

$$\text{URM}_1 = \frac{B_{13}}{B_{23}} = \frac{2}{1 - \sqrt{3} \tan(\theta)} \quad (16)$$

$$\text{URM}_2 = \frac{B_{12}}{B_{23}} = \frac{1 + \sqrt{3} \tan(\theta)}{1 - \sqrt{3} \tan(\theta)} \quad (17)$$

From the geometry and the equations, it is clear that we can obtain all the URM ratios that we can possibly get just by sweeping θ from 0 to 30 degrees. All other tilt angles will also map to the same URM range, so we only consider θ ranging from 0 to 30 degrees. Plotting URM ratios against θ , as θ varies from 0 to 30 degrees, Figure 15 gives us the following plot.

We note that the URM ratios approach infinity asymptotically as we approach 30 degrees, because B_{23} gets increasingly small, and reaches 0 at $\theta = 30$ degrees. It is imperative to decide what URM ratios to be actually used for any actual satellite geometry and configuration. For example, if the baselines are such that the ratio is 3.12648, do we use that actual ratio (and thus have lots of line segments), or do we choose an alternate URM ratio to do the projection? We seek to investigate this by performing the following experiment:

1. Change the tilt angle such that URM_1 is 3.35.
2. During the projection module, map the noisy points onto the line segments defined by URM_1 and URM_2 , where $\text{URM}_1 \in \{3.1, 3.2, 3.3, 3.4, 3.5, 3.6\}$, and $\text{URM}_2 = \text{URM}_1 - 1$.
3. After mapping onto the chosen URM values, find the mean RMS error in height.
4. Repeat for all other URM values, until the set is exhausted.

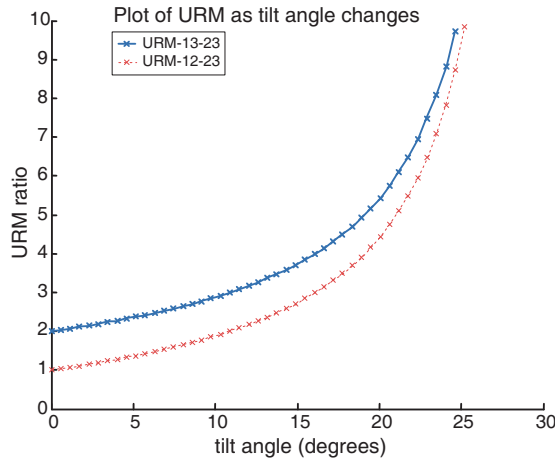


Figure 15. Plot of URM ratios as tilt angle changes.

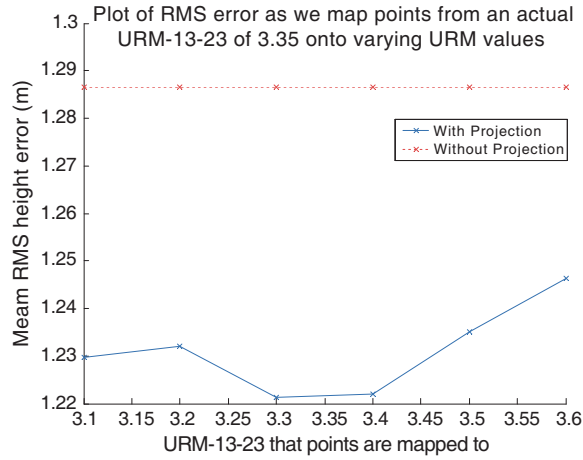


Figure 16. Illustration of RMS error as we map points onto different URM values.

We then plot the mean RMS errors in height as a function of URM_1 , and present the results in the Figure 16.

From Figure 16, we can see that we get the lowest RMS height errors when we map onto URM values closest to 3.35 (3.3, 3.4), and the results degrade as we map onto values further away from 3.35. This shows that we should always try to map onto URM values that are closest to the actual URM ratio. Intuitively, this makes sense, since the mapping process inherently disturbs the data and so might

introduce noise of its own as well, and mapping data points onto a URM value that is significantly different from the actual URM based on the satellite geometry will inevitably introduce more noise.

So, now we have the algorithm for 3-D Projection as follows:

1. From the geometry of the satellite configuration, determine the actual URM values.
2. Determine the URM values to be used for projection. Mathematically, this is:

$$\text{URM}_{\text{to-be-used}} = \frac{\lfloor 10 \cdot \text{URM}_{\text{actual}} \rfloor}{10}$$

It simply means rounding the actual URM value to the nearest 0.1.

3. Map the noisy points to line segments of the $\text{URM}_{\text{to-be-used}}$ values in 3-D space.
4. Continue with the height retrieval process using these newly corrected phase values.

Increasing levels of noise invariably introduces increasing errors in the heights retrieved from the phases of the interferogram. Using Projection method in tandem with other noise filtering techniques such as wavelet denoising or complex averaging [16], significant improvements can be expected. Using a satellite configuration with a more realistic of $\text{URM}_1 = 3.35$, we investigate the merits of 3-D Projection by finding the RMS height errors as we change the phase noise level. The results are shown in Figure 17.

From Figure 17, it is clear that 3-D projection does not fare worse than not-using Projection; in fact, for higher noise levels, the noise reduction capability of 3-D Projection is fairly significant. In the cases of when noise level is fairly low (between 0 and 40 degrees), it is inconclusive from the graph whether projection helps or hurts noise filtering. It is worth noting that even at a noise level of 0 degrees, there is still some height error. This is due to the fact that complex averaging is used as a denoising technique when the interferograms are retrieved. It has been shown that complex averaging does give much better results, but also inadvertently introduces errors when there is no noise.

We now look at the relationships among the satellite configuration, i.e., as the cartwheel is rotated through different angles, the amount of noise in the system, and the mean RMS errors in height. Fifty random and different values of URM (and thus 50 different satellite configurations) are picked from within the set in the set $[0, 30)$ degrees (which will provide us with any URM value in the set $[2, \infty)$). We vary

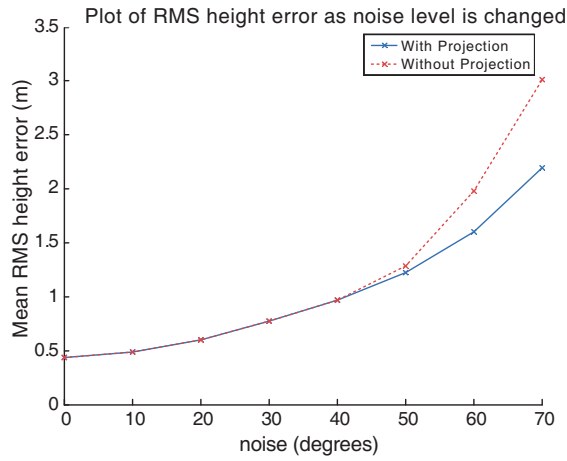


Figure 17. Illustration of how height errors change as noise level is increased.

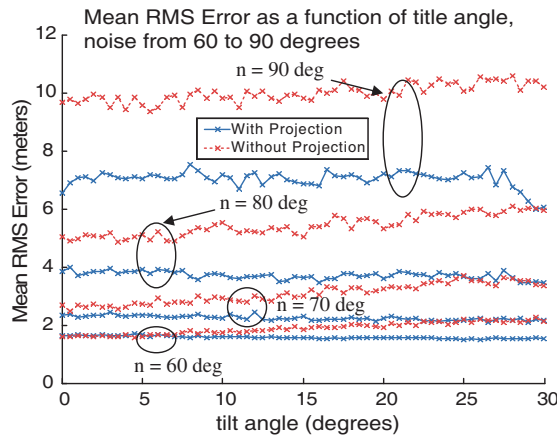


Figure 18. Illustration of how mean RMS height error changes as cartwheel is rotated and as noise in the system is changed.

noise values from 0 to 90 degrees to test for behavior of the different methods as noise increases. The results are shown in Figure 18.

From Figure 18, the following is clear:

1. At low noise levels, 3-D Projection even in the general case of non-integer URM ratios still does not introduce more error than if we do no projection at all.
2. At higher noise levels, 3-D Projection fares significantly better in terms of RMS height errors.

3. At tilt angles close to 30 degrees, the RMS error due to 3-D Projection seems to decrease significantly. This can be reasoned as follows: Even though there is the rapidly shrinking B_{23} , which directly leads to a huge URM_{13-23} and URM_{12-23} and thus short noise distances, this effect does not show itself because of weighted averaging.

5. CONCLUSION

By adding a third antenna to the InSAR system, Unambiguous Range Magnification (URM) is possible, with the URM ratio being the ratio of baselines. Since there are 3 pairs of satellites now, there would be 2 independent URM ratios (and hence 2 independent slopes). 2D Projection is a technique based on the underlying geometry of the satellites to reduce the noise in the system. It is able to reduce the effects of noise on the unwrapped phases. In contrast, 3D Projection takes into account of the consistency offered by all 3 satellites, and thus achieves even better results than 2D Projection. We can obtain all URM ratios in the set $[2, \infty)$ by rotating the satellites in the cartwheel configuration from 0 to 30 degrees. In addition, simply mapping all URM ratios to the set of $\{2.1, 2.2, 2.3, \dots, 3.1, 3.2, \dots\}$ gives us better results than not doing the mapping at all. 3-D Projection fares much better than 2-D Projection in almost all noisy cases across all tilt angles. Specifically, at tilt angles close to 30 degrees, the improvement is the most significant. This is because mathematically, 2-D Projection is simply a special case of 3-D Projection. Thus, we can reap all benefits of 2-D Projection using 3-D Projection.

ACKNOWLEDGMENT

The author would like to acknowledge the support of Mitsubishi Electric Corporation.

REFERENCES

1. Ghalia, D. C. and L. A. Romero, "Robust two-dimensional weighted and unweighted phase unwrapping that uses fast transforms and iterative methods," *Journal of the Optical Society of America*, Vol. 11, 107–117, Jan. 1994.
2. Lombardini, F., "Absolute phase retrieval in a three-element synthetic aperture radar interferometer," *CIE International Conference of Radar Proceedings*, 309–312, Oct. 1996.

3. Hunt, B., "Matrix formulation of the reconstruction of phase values from phase differences," *American Journal of Optical Society*, Vol. 69, 394–399, 1979.
4. Trouve, E., J. M. Nicholas, and H. Maitre, "Improving phase unwrapping techniques by the use of local frequency estimates," *IEEE Transactions on Geoscience and Remote Sensing*, Vol. 36, 1963–1972, Nov. 1999.
5. Liu, D., Y. Du, G. Sun, W.-Z. Yan, and B.-I. Wu, "Analysis of insar sensitivity to forest structure based on radar scattering model," *Progress In Electromagnetics Research*, PIER 84, 149–171, 2008.
6. Singh, D. and A. Kathpalia, "An efficient modeling with GA approach to retrieve soil texture, moisture and roughness from ERS-2 SAR data," *Progress In Electromagnetics Research*, PIER 77, 121–136, 2007.
7. Nie, X., D.-Y. Zhu, and Z.-D. Zhu, "Application of synthetic bandwidth approach in SAR polar format algorithm using the deramp technique," *Progress In Electromagnetics Research*, PIER 80, 447–460, 2008.
8. Sabry, R. and P. W. Vachon, "Advanced polarimetric synthetic aperture radar (SAR) and electro-optical (EO) data fusion through unified coherent formulation of the scattered EM field," *Progress In Electromagnetics Research*, PIER 84, 189–203, 2008.
9. Tan, C. P., J. Y. Koay, K. S. Lim, H. T. Ewe, and H. T. Chuah, "Classification of multi-temporal SAR images for rice crops using combined entropy decomposition and support vector machine technique," *Progress In Electromagnetics Research*, PIER 71, 19–39, 2007.
10. Koo, V. C., C. S. Lim, and Y. K. Chan, "iSIM — An integrated SAR product simulator for system designers and researchers," *Journal of Electromagnetic Waves and Applications*, Vol. 21, No. 3, 313–328, 2007.
11. Cho, B. L. and Y. S. Kim, "Multilook coherence estimation using adaptive weighted window in interferometric SAR," *Journal of Electromagnetic Waves and Applications*, Vol. 21, No. 3, 359–365, 2007.
12. Lim, T. S., V. C. Koo, H. T. Ewe, and H. T. Chuah, "High-frequency phase error reduction in SAR using particle swarm of optimization algorithm," *Journal of Electromagnetic Waves and Applications*, Vol. 21, No. 6, 795–810, 2007.
13. Xu, W., E. C. Chang, L. K. Kwoh, H. Lim, and W. C. A. Heng, "Phase unwrapping of SAR interferograms with multi-frequency

- or multi-baseline,” *International Geoscience and Remote Sensing Symposium*, 730–732, 1994.
14. Xu, H., Y. Zhou, and C. Li, “Analysis and simulation of spaceborne SAR interferometric baseline,” *CIE International Conference of Radar Proceedings*, 639–643, Oct. 15–18, 2001.
 15. Wong, W., “Synthetic aperture radar interferometry with 3 satellites,” Paper for Master of Science, MIT, Jun. 2005.
 16. Braunisch, H., B.-I. Wu, and J. A. Kong, “Phase unwrapping of SAR interferograms after wavelet denoising,” *Proc. IEEE Int. Geosci. Remote Sensing Symp. (IGARSS)*, Vol. 2, 752–754, Honolulu, Jul. 24–28, 2000.